JACS
JOURNAL OF THE AMERICAN CHEMICAL SOCIETY
Article
pubs.acs.org/JACS

Superhard Rhenium/Tungsten Diboride Solid Solutions

Andrew T. Lech,[†,⊥] Christopher L. Turner,[†,⊥] Jialin Lei,[†] Reza Mohammadi,[‡] Sarah H. Tolbert,[†,§,∥] and Richard B. Kaner*[,†,§,∥]

[†]Department of Chemistry and Biochemistry, [§]Department of Materials Science and Engineering, [∥]California NanoSystems Institute (CNSI), University of California, Los Angeles, California 90095, United States

[‡]Department of Mechanical and Nuclear Engineering, Virginia Commonwealth University, Richmond, Virginia 23284, United States

ABSTRACT: Rhenium diboride (ReB_2), containing corrugated layers of covalently bonded boron, is a superhard metallic compound with a microhardness reaching as high as 40.5 GPa (under an applied load of 0.49 N). Tungsten diboride (WB_2), which takes a structural hybrid between that of ReB_2 and AlB_2, where half of the boron layers are planar (as in AlB_2) and half are corrugated (as in ReB_2), has been shown not to be superhard. Here, we demonstrate that the ReB_2-type structure can be maintained for solid solutions of tungsten in ReB_2 with tungsten content up to a surprisingly large limit of nearly 50 atom %. The lattice parameters for the solid solutions linearly increase along both the *a*- and *c*-axes with increasing tungsten content, as evaluated by powder X-ray and neutron diffraction. From micro- and nanoindentation hardness testing, all of the compositions within the range of 0−48 atom % W are superhard, and the bulk modulus of the 48 atom % solid solution is nearly identical to that of pure ReB_2. These results further indicate that ReB_2-structured compounds are superhard, as has been predicted from first-principles calculations, and may warrant further studies into additional solid solutions or ternary compounds taking this structure type.

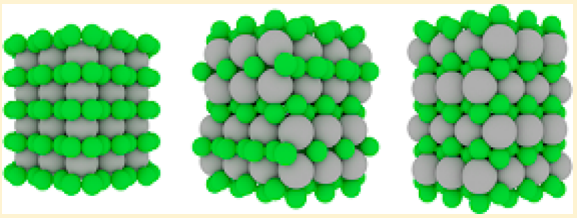

INTRODUCTION

For the past few years, transition metal diborides have attracted a great deal of attention among materials researchers due to their combination of outstanding physical properties, such as metallic electrical conductivity, high incompressibility, high shear strength, and exceptionally high hardness.[1] All of these attributes are desirable in materials for structural and engineering compounds and indicate that diborides may be suitable replacements for current metal carbides in next-generation cutting tools.[2] Generally, these properties are also correlated: a high bulk modulus (incompressibility) appears to be a necessary,[3] if not sufficient,[4] predictor of high hardness.[5] The design philosophy pursued to take advantage of this correlation has attempted to force highly incompressible metals to also become resistant to shear through the introduction of covalent bonds.[6,7] Boron is a small, highly bonded[8] element that is capable of forming bonds to metals,[9] thus creating transition metal borides.

As such, we have previously shown that rhenium diboride (ReB_2) is one of the hardest metallic compounds known, with a Vickers hardness under a low applied load (0.49 N) reaching as high as 40.5 GPa.[10] This value is above the arbitrary threshold[3] of 40 GPa commonly accepted for superhard compounds, and it gives ReB_2 the distinction of being one of the first superhard metals identified.[11] We have since furthered the scope of our attention to even higher borides, such as WB_4, which we have shown to have the potential to become even significantly harder, achieving a Vickers hardness of up to 57.3 GPa under a 0.49 N load when appropriate solid solutions with metals such as Ta, Mn, and Cr are formed.[12] However, it was in the course of our work with tungsten tetraboride that we first noticed a peculiarity in the interaction of rhenium and tungsten in the presence of excess boron.[13] While the addition of rhenium was found to increase the hardness of WB_4, this effect was due most apparently to a fine dispersion of ReB_2 found in the arc-melted ingots. Intriguingly, the lattice parameters of ReB_2 in the composite sample were found to be somewhat larger than those of pure ReB_2, implying the formation of a ReB_2/WB_2 solid solution.

While WB_2 does not take the ReB_2 structure under any known conditions, the native structure of WB_2 (often referred to as the W_2B_4 structure) equally incorporates elements found in two parent types: those of AlB_2 (*P6/mmm*) and ReB_2 ($P6_3/mmc$) (Figure 1). Given the hybrid nature of the WB_2 structure, it seems intuitive that tungsten might show some ability to form mixed-metal ternaries and solid solutions with materials that take *either* the ReB_2 *or* AlB_2 structure type. In agreement with this idea, solid solutions of tungsten with metal borides taking the AlB_2 structure type (e.g., TiB_2) have been reported.[14] Furthermore, it is known that some tungsten-containing ternaries, such as $W_{0.5}Ru_{0.5}B_2$ and $W_{0.5}Os_{0.5}B_2$, may take the ReB_2 structure type, as first identified by Rogl et al.[15−17] and recently revisited by Zeiringer and Rogl et al.[18] Unfortunately, little is historically reported about the solid solubility of tungsten in ReB_2 itself, save for a lone mention by Kuz'ma et al. in a Soviet-era phase diagram.[19]

Additionally, since our original identification of superhardness in ReB_2, an increasingly large number of theoretical works have appeared in the literature with calculations of hardness using first-principles methods for metal borides of this type.[20−36]

Received: August 17, 2016
Published: October 10, 2016

DOI: 10.1021/jacs.6b08616
J. Am. Chem. Soc. 2016, 138, 14398−14408

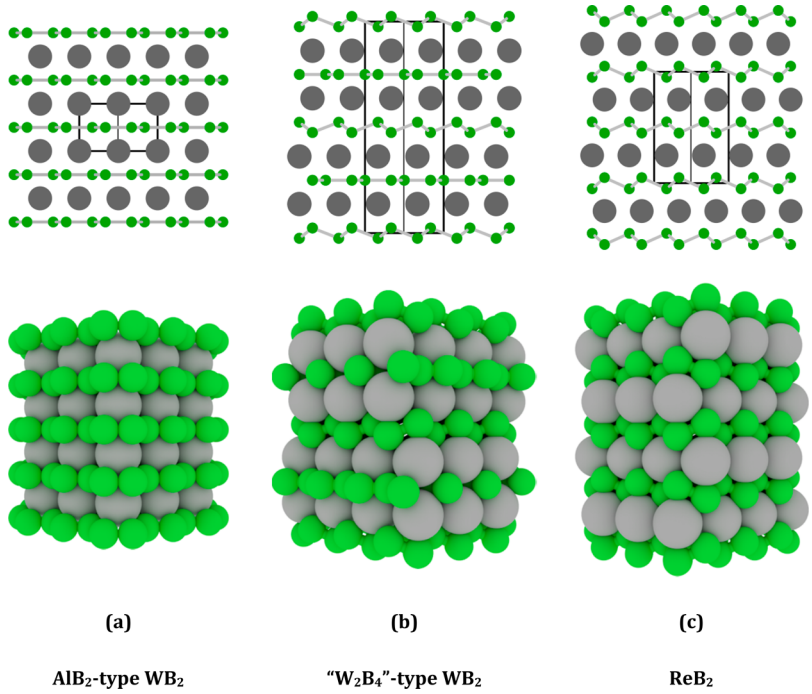

Figure 1. Comparison of the structures of several diborides structure types. Top: Schematic representation of the borides, normal to the [111] crystallographic plane, emphasizing the stacking sequence of the metal atoms. The unit cell for each structure is bounded by the black box. Bottom: Space-filling atomic models of the above structures shown along the same viewing direction, emphasizing the interstitial nature of the atomic filling of boron. All structures are drawn to scale.

Several of these works have made claims to predict the already measured and reported properties of previously synthesized materials, but there are few examples of true predictions followed by experimental validation. Therefore, it is as yet unclear to what extent the experimentalist might find these sorts of calculations to be a useful guidance for the creation of new compounds with reliably predetermined properties and to what extent these works represent *post hoc* rationalization of properties that have already been determined. A few of these works, however, have made predictions for the properties of solid solutions that are hypothetically synthesizable using ordinary techniques but for which the properties have not yet been reported. Included among these are several works making predictions for ReB_2-structured WB_2 and for rhenium/tungsten diboride solid solutions.[20,23,31,32,36−38] As a result, experimental realization of such a system would be an ideal test of these theoretical predictions.

For the reasons mentioned above, solid solutions employing WB_2 as either the host or guest component are worthy systems of study for hard-materials research. From a crystallochemical perspective, a hybrid structure of WB_2 and ReB_2 should lead to relatively straightforward transformations to other structure types with presumably tunable lattice parameters and properties. From the perspective of the experimentalist, wary of the reliability of guidance taken from theory, it makes an interesting test for the accuracy that can be expected from predictions of this kind.

Here, we thus report the successful synthesis of solid solutions of ReB_2 and WB_2 that take on the superhard ReB_2 structure type. Additionally, we report the hardness of these solid solutions and the structural evolution occurring in the ReB_2 lattice as a result of the dissolution of tungsten. Thus far, to our knowledge, the work presented here would appear to be the only detailed experimental study of properties of solid solutions of tungsten and rhenium diborides. We have found that, while tungsten causes a monotonic increase in the lattice parameters of ReB_2, all of the solid solutions maintain superhardness under low loads and that the hardness of ReB_2 is significantly increased by ca. ≈ 17% for small additions of tungsten metal. Moreover, the bulk modulus of a nearly equimolar W/Re solid solution is basically identical to that of pure ReB_2. This work further allows comparisons of these properties (e.g., hardness) to selected theoretical predictions from the literature to be made, from which we conclude that first-principles hardness models may indeed provide qualitative guidance for the experimentalist in the search for hard metallic phases.

MATERIALS AND METHODS

Powders of tungsten (99.95%, Strem Chemicals, USA), rhenium (99.99%, CERAC Inc., USA), and amorphous boron (99+%, Strem Chemicals, USA) for X-ray diffraction or crystalline ^{11}B (99.9%, 98.5% ^{11}B enriched, Ceradyne, USA) for neutron diffraction were uniformly mixed in the ratio M:B = 1:2.25 using an agate mortar and pestle. For solid solutions, tungsten was substituted for rhenium at concentrations in the range of 0.5−48.0 atom % such that the total M:B ratio was maintained. The slight excess of boron is required to counteract its evaporation during the process of arc melting and to prevent the formation of lower borides of tungsten. Each mixture was consolidated into a 12 mm, ∼500 mg pellet by means of a hydraulic press (model 3851, Carver, USA) under a pressure of ∼562 MPa. The pellets were then placed in an arc-melting furnace consisting of a water-cooled copper hearth/anode and a nonconsumable tungsten cathode. Subsequently, the atmosphere of the furnace was purged several times with ultra-high-purity argon. After removing trace gases in the system by melting several small chips of a titanium/zirconium alloy, an ∼100 A dc current was applied to the samples, melting them. The fused ingots were then flipped and subjected to the electric arc two additional times in order to ensure homogeneity. Once cooled, the ingots were bisected using a sinter-bonded diamond lapidary sectioning saw (South Bay Technology Inc., USA). One-half of each ingot was crushed to a powder

DOI: 10.1021/jacs.6b08616
J. Am. Chem. Soc. 2016, 138, 14398−14408

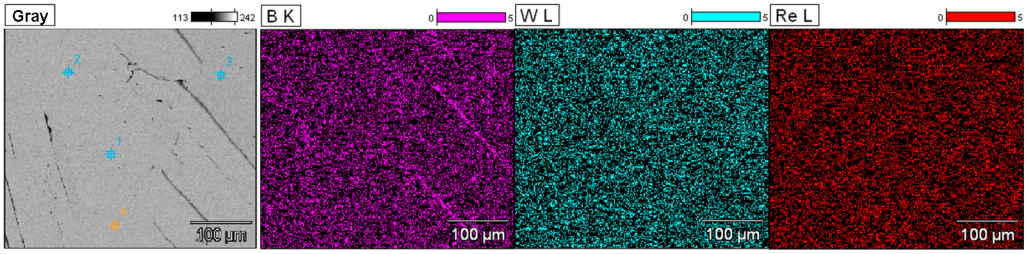

Figure 2. Elemental map for an $Re_{0.52}W_{0.48}B_2$ sample, indicating the composition and location of boron (K line), tungsten (L line), and rhenium (L line). The four randomly selected areas for composition analysis (from Table 1) are shown in the gray image. The average grain size is less than 100 μm, and the distribution of tungsten and rhenium is found to be uniform throughout the grains.

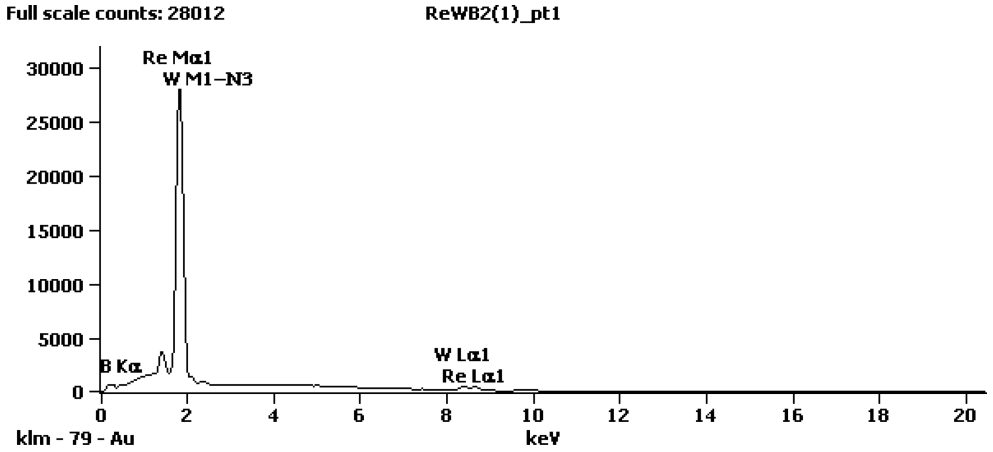

Figure 3. EDS spectra of an $Re_{0.52}W_{0.48}B_2$ sample. Spot 1 (gray image in Figure 2) spectra was chosen, but all spectra are nearly identical when overlaid; Table 1 shows the difference in composition among the four randomly selected spots.

(−325 mesh) using a Plattner-style, hardened tool-steel mortar (model H-17270, Humboldt Mfg. Co., USA). The powdered samples were washed three times with 1 M HCl to remove impurities introduced from the steel grinding equipment.

Powder samples for X-ray diffraction (XRD) were placed in a flat-stage holder, and the sample surface was flattened by removing excess powder across scans. All X-ray data were collected on an X'Pert Pro Bragg-Bentano geometry powder diffraction system (PANalytical, Netherlands), employing nickel filtered $Cu_{K\alpha}$ radiation ($\lambda_{K\alpha1}$ = 1.540593 Å, $\lambda_{K\alpha2}$ = 1.5444274 Å),[39] 0.04 rad Soller slits, and X'Celerator position sensitive detector. The collected data were subjected to least-squares refinement using the EXPGUI[40] front-end to the GSAS[41] Rietveld refinement software package, from which the lattice parameters were extracted. Samples annealed at 1300 K for 24 h prior to grinding were found to give results identical to unannealed (as-synthesized) samples.

To verify the results from X-ray diffraction and to assess any changes in the atomic coordinates of boron in the ReB_2 structure, samples of ReB_2 and $Re_{0.52}W_{0.48}B_2$ enriched in ^{11}B were subjected to neutron time-of-flight (TOF) powder diffraction at the HIPPO Beamline at LANSCE (Los Alamos Neutron Science Center, Los Alamos National Lab, Los Alamos NM). For these experiments, the samples were annealed at 1300 K for 24 h prior to their coarse grinding (−220 mesh) and subsequent washing with 1 M HCl. The powders were placed in sealed vanadium "cans" and subjected to water-moderated thermal neutrons collimated to 1 cm diameter for a total time of 1 h each while their diffraction patterns were collected by an array of ^3He scintillation-counter panels arranged at 144 and 90° about the sample. The neutron diffraction data were refined from the high-resolution 144° backscattering panel using the EXPGUI[40] and GSAS[41] Rietveld refinement software packages.

Hardness data were obtained via micro- and nanoindentation of the unground half of each ingot. Prior to hardness testing, the samples were first cold-mounted in epoxy (Allied High Tech Products Inc.) and polished to an optically flat surface using a tripodal polisher (South Bay Technology Inc., USA) with SiC polishing papers (120−1200 grit, Allied High Tech Products Inc., USA) followed by diamond films (30−0.5 μm, South Bay Technology Inc., USA).

Microindentation was performed by the Vickers method using a MicroMet 2103 microhardness tester (Buehler GmBH, Germany) with a pyramid diamond tip. Indentations were made under five loads ranging from 0.49 to 4.9 N with a dwell time of 15 s. To ensure accuracy, at least nine randomly chosen spots separated by over 100 μm were chosen for indentation at each load. The results reported here represent the averages of these points. The lengths of the diagonals of the indents were then measured with a high-resolution Zeiss Axiotech 100HD optical microscope (Carl Zeiss Vision GmbH, Germany), and eq 1 was used to obtain Vickers microindentation hardness values (H_v)

$$H_v = \frac{1854.4P}{d^2} \quad (1)$$

where P is the applied load (in N) and d is the arithmetic mean of the diagonals of the indent (in μm).

Nanoindentation was performed using an MTS Nano Indenter XP (MTS, USA) with a Berkovich diamond tip. After calibration of the indenter with a standard silica block, the samples were indented automatically to a depth of 950 nm at 20 "randomly" predetermined points, and the resulting load versus displacement plots were averaged. The nanoindentation hardness of the material may be found based on the shape of the loading and unloading curves by the method of Oliver and Pharr[42] using eq 2

$$H = \frac{P_{max}}{A} \quad (2)$$

where H, P_{max}, and A are nanoindentation hardness, peak indentation load, and projected area of the hardness impression, respectively.[42]

Superhard materials tend to possess a high bulk modulus in addition to high hardness. The incompressibility of $Re_{0.52}W_{0.48}B_2$ was measured using synchrotron-based radial X-ray diffraction in a diamond anvil cell (DAC).[43] The high pressure experiments were performed in an angle-

DOI: 10.1021/jacs.6b08616
J. Am. Chem. Soc. 2016, 138, 14398−14408

dispersive geometry at beamline 12.2.2 of the Advanced Light Source (ALS, Lawrence Berkeley National Lab). Polycrystalline $Re_{0.52}W_{0.48}B_2$ was ground to a powder with a grain size of <20 μm and then loaded into a ~60 μm diameter sample chamber in a boron gasket. This gasket (~400 μm in diameter and ~70 μm in thickness) was embedded in a small rectangular Kapton sheet. A piece of ~25 μm diameter Pt foil was placed on top of the sample to serve as a pressure internal standard. No pressure-transmitting medium was used in order to create a non-hydrostatic environment in the DAC. A monochromatic X-ray beam with a wavelength of 0.4959 Å and size of 20 × 20 μm was passed through the sample perpendicular to the loading axis. The 2D diffraction image was collected with the FIT2D[44] program at a step of ~4 GPa after calibration of the detector distance and orientation using a LaB_6 standard.

Thermal stability of the powder samples (−325 mesh) was studied in air (nonmedical) using a Pyris Diamond thermogravimetric/differential thermal analyzer module (TG-DTA, PerkinElmer Instruments, USA). Samples were heated to 200 °C at a rate of 20 °C/min and soaked at this temperature for 10 min to remove water vapor. They were then heated to 1000 °C at a rate of 2 °C/min and held at this temperature for 120 min. The samples were then air cooled at a rate of 5 °C/min. X-ray diffraction was carried out on the powders after cooling to determine the resulting phases.

In order to verify the elemental composition, beyond XRD analysis, an $Re_{0.52}W_{0.48}B_4$ sample was analyzed on an FEI Nova 230 high-resolution scanning electron microscope (FEI Co., USA), utilizing an UltraDry EDS detector (Thermo-Scientific Inc., USA); four points were randomly selected for elemental spectra, and elemental composition maps were produced, as seen in Figures 2 and 3. The elemental compositions matched, within error, to the stoichiometry of the sample, and there was no evidence of elemental impurities within the sample (potentially introduced through the synthesis process), as seen in Table 1. To assess the phase stability of the solid solutions, several samples were thermally annealed over a period of 24 h at a temperature of 1300 K under flowing high-purity argon in a Lindberg/Blue M Mini Mite laboratory tube furnace (Thermo-Scientific Inc., USA). The samples were crushed and analyzed by X-ray diffraction using the above procedure. The lattice parameters differed trivially from samples subjected only to arc melting, although the fwhm for the peaks was somewhat reduced, indicating the elimination of some lattice strain.

Table 1. Energy-Dispersive X-ray Spectroscopy of $Re_{0.52}W_{0.48}B_2$[a]

	B−K	W−M	Re−M
ReWB2_pt1	61.27 ± 1.02	19.82 ± 0.22	18.91 ± 0.23
ReWB2_pt2	61.58 ± 1.04	17.44 ± 0.24	20.97 ± 0.33
ReWB2_pt3	60.80 ± 1.05	20.70 ± 0.85	18.50 ± 1.03
ReWB2_pt4	62.18 ± 1.09	19.68 ± 0.82	18.14 ± 1.00

[a]Energy-dispersive X-ray spectroscopy of randomly selected points of an $Re_{0.52}W_{0.48}B_2$ sample, in atom %. The locations selected correspond to Figure 2, whereas Figure 3 provides a representative spectrum. The consistent ratio of metals (W:Re) is nearly 1:1, within the detection limit of the instrument.

RESULTS AND DISCUSSION

As one might predict on the basis of the WB_2 structure, consisting of one-half ReB_2-type HCP-type layers and one-half AlB_2-type simple hexagonal layers, the maximum solubility of tungsten in ReB_2 is nearly 50%. A sample powder X-ray diffraction pattern for the highest concentration used in this study (48 atom % W) is given in Figure 4. The lattice parameters, unit cell volume, and c/a axial ratios for a selection of solid solutions synthesized for this study are listed in Table 2. Both the a- and c-axes are expanded by incorporation of tungsten into the ReB_2 structure and monotonically increased in absolute value as a function of tungsten concentration. The near-perfect linear trends observed (Figures 5 and 6) would be predicted by strict adherence to Vegard's law if a hypothetical ReB_2-type tungsten diboride existed. By extrapolating the curves in Figure 6, the lattice parameters for such a hypothetical ReB_2-type WB_2 compound may be estimated as a = 2.9159 Å and c = 7.7486 Å. These values can be compared to a = 2.9002 Å and c = 7.4759 Å for pure ReB_2, resulting in a total volume increase of approximately 4.64% in the hypothetical W analogue.

Microhardness data are presented in Figure 7. Small additions of tungsten in the range of 0.5−2 atom % have a relatively large and immediate impact on the hardness of ReB_2, which increases from 40.5 ± 2.8 GPa (1% W addition) to 47.8 ± 3.5 GPa (0.5% W addition) at low load (0.49 N) and from 29.3 ± 0.8 GPa (1% W addition) to 33.9 ± 0.7 GPa (0.5% W addition) at high load (4.9 N). The addition of larger amounts of tungsten produces less dramatic changes, although all of the solid solutions are at least slightly harder than pure ReB_2. Calculated hardness values for all of the compositions tested are given in tabular form with their corresponding estimated standard errors in Table 3.

The nanoindentation data (Figure 8) largely corroborate the Vickers microhardness data. As the curves heavily overlap for the samples of various concentrations (again emphasizing their similarity in hardness), the inset shows an expanded view of the region of low load where, again, small concentrations of tungsten are found to have a disproportionately large impact on the hardness of ReB_2 even though all concentrations are at least as hard as pure ReB_2. A maximum hardness of 48.12 GPa was found for 0.5% W in ReB_2 at a displacement of 55.4 nm (load of 2.63 mN) compared to 43.99 GPa at 64.0 nm (3.16 mN load) for pure ReB_2. Likewise, all of the tungsten-containing solid solutions synthesized maintained hardness values greater than 40 GPa until well over 200 nm of penetration depth. Table 4 summarizes the hardness values obtained at various penetration depths as well as the average hardness found over the range from 60 to 900 nm for the various compositions tested. All of the compositions tested were superhard.

To examine any crystallographic effects of dissolving tungsten in the ReB_2 structure, time-of-flight (TOF) neutron powder diffraction data were obtained for the highest composition obtained (48 atom % W) as well as for pure ReB_2. The background-subtracted, Rietveld-refined powder diffraction patterns are depicted in Figure 9, and the relevant crystallographic data can be found in Tables 5 and 6. The neutron diffraction data for ReB_2 are in excellent agreement with those observed by Frotscher et al. (cf. a = 2.90059 Å c = 7.47745 Å versus our a = 2.900468 Å and c = 7.47734 Å).[45] There is no evidence for preferential site orientation or secondary phases. The fit to the solid solution sample is nearly as good as that for pure ReB_2 (χ^2 = 1.731 versus 2.023) and potentially could be improved toward parity if the thermal parameters were separately refinable for the Re and W atoms without correlation. The discrepancy in lattice parameters between the neutron and X-ray diffraction samples is most likely due to a slight difference in zero-point calibration between the two machines. The overall trend in parameters is, however, maintained, as can be seen from the c/a axial ratios shown in Table 2, where the difference between the ratios calculated by the two techniques is less than the error that would be introduced by a discrepancy of 0.25 atom % in tungsten composition (calculated from the trend in Figure 5).

The volume of the unit cell as a function of pressure was measured in the DAC under nonhydrostatic conditions. Data were measured at φ = 54.7°, where φ is the angle between the

DOI: 10.1021/jacs.6b08616
J. Am. Chem. Soc. 2016, 138, 14398−14408

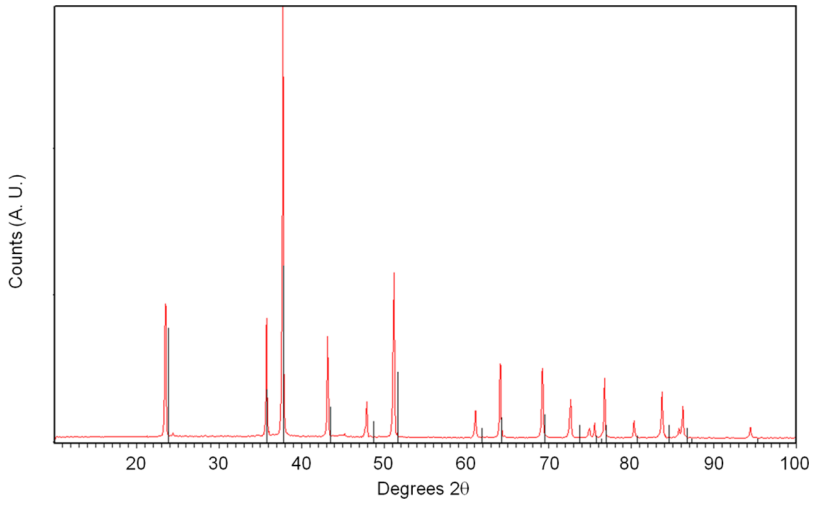

Figure 4. Sample X-ray diffraction pattern of a specimen containing 48 atom % tungsten in ReB_2 showing the full pattern shifting of peaks. Peaks having greater {00*l*} character are shifted to a more noticeable extent due to the greater sensitivity of the *c*-axis to the solubility of tungsten. The black stick pattern represents where the diffraction peaks appear for pure ReB_2.

Table 2. Lattice Parameters, Cell Volumes, and Axial Ratios for the W/ReB_2 Solid Solutions[a]

composition	*a* parameter (Å)	*c* parameter (Å)	volume (Å^3)	*c*/*a* ratio
ReB_2 (X-ray)	2.90016(1)	7.47591(8)	54.455	2.5778
ReB_2 (neutron)	2.900468(24)	7.47734(10)	54.477	2.5780
$Re_{0.995}W_{0.005}B_2$	2.9006(7)	7.4799(2)	54.504	2.5787
$Re_{0.95}W_{0.05}B_2$	2.9014(5)	7.4917(2)	54.618	2.5821
$Re_{0.90}W_{0.10}B_2$	2.9019(3)	7.5056(5)	54.738	2.5864
$Re_{0.80}W_{0.2}B_2$	2.9033(8)	7.5315(6)	54.981	2.5941
$Re_{0.70}W_{0.30}B_2$	2.9046(7)	7.5573(2)	55.220	2.6018
$Re_{0.60}W_{0.40}B_2$	2.9065(7)	7.5884(1)	55.519	2.6108
$Re_{0.52}W_{0.48}B_2$ (X-ray)	2.9076(9)	7.6076(8)	55.701	2.6164
$Re_{0.52}W_{0.48}B_2$ (neutron)	2.909085(21)	7.61009(10)	55.774	2.6160

[a]Numbers in parentheses represents the uncertainty of the preceding least-significant digit.

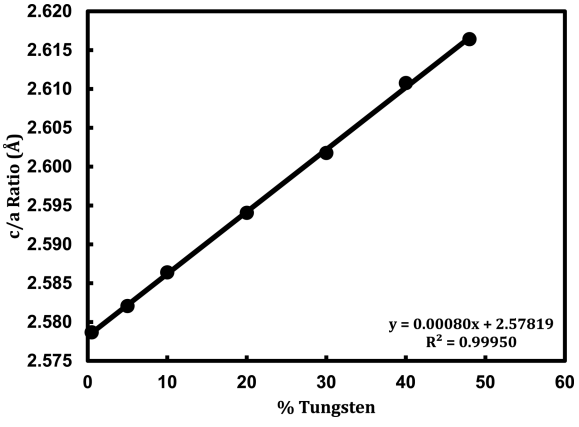

Figure 5. Plot of the calculated axial ratio for the ReB_2 structured solid solutions versus tungsten content in atomic percentage. As both values increase monotonically, the axial ratio increases monotonically as well. The linear best-fit equation is given in the lower right corner.

diffracting plane normal and the maximum stress axis. It is believed that the volume measured at $\varphi = 54.7°$ reflects the compression behavior due to the hydrostatic component of stress.[46−48] The compression data were then fit to the second order Birch−Murnaghan equation of state (eq 3) as a function of the normalized pressure (F_v, eq 5) and Eularian strain (f_v, eq 4),[49,50] as seen below

$$P = 1.5K_0[(V/V_0)^{-7/3} - (V/V_0)^{-5/3}] \quad (3)$$

$$f_v = \frac{1}{2}\left(\left(\frac{v_0}{v}\right)^{2/3} - 1\right) \quad (4)$$

$$F_v = \frac{P}{3f_v(1 + 2f_v)^{2.5}} \quad (5)$$

Here, the pressure (P) is provided by the pressure standard within the test cell, and the change in volume (V_0 at ambient pressure and V under pressure) were determined experimentally. Together, these allow for the calculation of the normalized pressure (F_v) and the Eulerian strain (f_v). As seen in Figure 10, the solid line yields a bulk modulus of 365 ± 4 GPa at ambient pressure with the pressure derivative fixed at 4. This value is higher than WB_2 (K_0 = 349 GPa)[51] and within error of pure ReB_2 (K_0 = 367 GPa),[52] emphasizing the key role of the ReB_2 structure type in determining the mechanical properties of these solid-solution-based materials. Note that deviations from linearity at low pressures are common and are likely due to incomplete compression of the sample and thus deviation in the pressure experienced by the sample and the pressure calibrant. The volume compression as a function of pressure is collected, advantageously, through radial diffraction; the X-ray beam runs parallel to the culet of the diamond. In this instance, hydrostatic conditions are not required because the diffraction peaks collected contain both the high and low stress directions. Therefore, hydrostatic conditions are not necessarily assumed, and the hydrostatic changes are calculated directly from the nonhydrostatic data at the magic angle (54.7°). Truly hydrostatic and nonhydrostatic/magic angle data give results that have strong agreement, and as such, either may be used to calculate the bulk modulus of a new material.

Thermogravimetric analysis data are presented in Figure 11. These data show little difference in thermal stability of the solid solutions versus data previously published for ReB_2, where

DOI: 10.1021/jacs.6b08616
J. Am. Chem. Soc. 2016, 138, 14398−14408

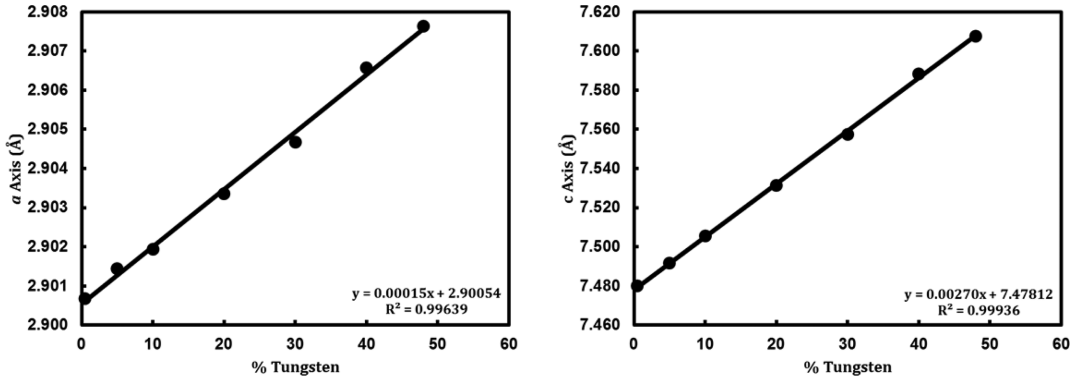

Figure 6. Plots of the measured (a) *a*-axis and (b) *c*-axis for the ReB_2 structured solid solutions versus tungsten content in atomic percentage. For both axes, the increase is virtually monotonic, but the rate of change in the *a*-axis parameter is significantly less than that seen for the *c*-axis. Linear best-fit equations are shown in the lower right corners. The unconstrained intercepts agree well with the measured lattice parameters for pure ReB_2.

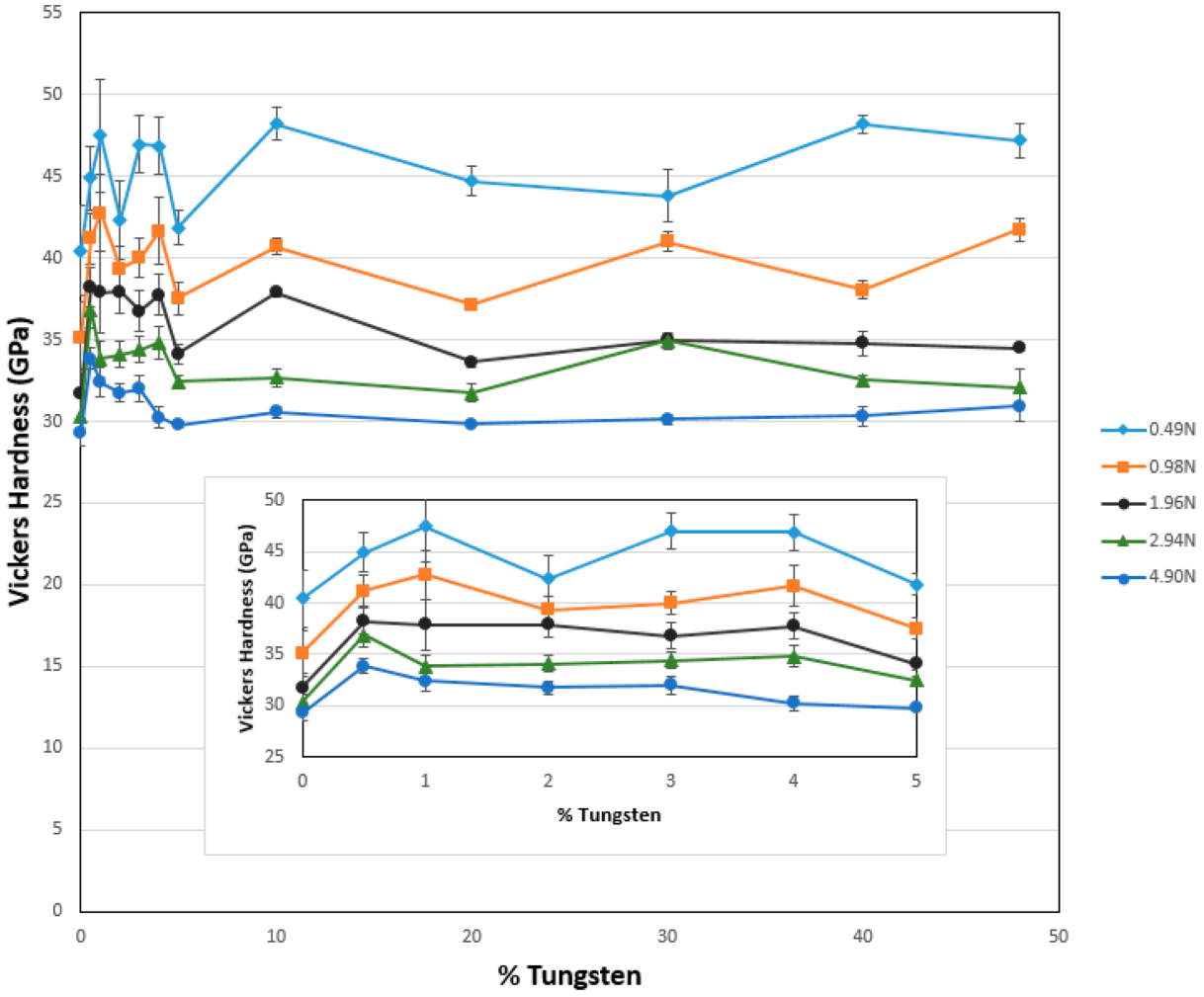

Figure 7. Vickers microindentation hardness versus metal-basis atomic composition of tungsten for various ReB_2-based solid solutions. Each indentation load is represented from a separate line in the plot. The hardness is dramatically increased with small additions of tungsten atoms; the effect rapidly diminishes as higher solid solubility is reached, with the plot becoming nearly flat for all loads for every concentration of tungsten from 10 to 48 atom %. Inset: Cropped view of the hardness enhancement from 0−5 atom % W addition.

oxidation of samples began at approximately the same temperature (≈500 °C).[10] The qualitative difference between the tungsten-containing samples and pure ReB_2 is an initial rise in mass before the steep drop, which may be ascribed to the formation of WO_3 or a mixed oxide of W/ReO_3 before the temperature is sufficiently hot for the sublimation of Re_2O_7. X-ray diffraction of the end product (a yellow, glassy microcrystalline mass) corroborates this hypothesis by confirming the

DOI: 10.1021/jacs.6b08616
J. Am. Chem. Soc. 2016, 138, 14398−14408

Table 3. Summary of Vickers Microhardness Data

	Vickers hardness (GPa)				
composition	0.49 N	0.98 N	1.96 N	2.94 N	4.90 N
ReB_2	40.45 ± 2.79	35.08 ± 2.21	31.73 ± 1.49	30.30 ± 0.74	29.31 ± 0.77
0.5% W	44.89 ± 1.94	41.19 ± 1.56	38.24 ± 1.21	36.85 ± 1.13	33.85 ± 0.69
1% W	47.47 ± 3.49	42.75 ± 2.39	37.86 ± 2.50	33.81 ± 1.07	32.40 ± 0.92
2% W	42.31 ± 2.38	39.35 ± 1.32	37.91 ± 1.31	34.10 ± 0.77	31.74 ± 0.57
3% W	46.96 ± 1.77	40.00 ± 1.17	36.75 ± 1.28	34.41 ± 0.83	31.97 ± 0.82
4% W	46.86 ± 1.71	41.65 ± 2.01	37.75 ± 1.28	34.82 ± 1.02	30.24 ± 0.66
5% W	41.83 ± 1.06	37.51 ± 1.03	34.11 ± 0.56	32.45 ± 0.38	29.79 ± 0.20
10% W	48.18 ± 1.01	40.69 ± 0.47	37.87 ± 0.25	32.66 ± 0.59	30.58 ± 0.34
20% W	44.69 ± 0.89	37.15 ± 0.37	33.62 ± 0.32	31.72 ± 0.54	29.81 ± 0.09
30% W	43.79 ± 1.58	40.98 ± 0.60	34.99 ± 0.35	34.92 ± 0.48	30.12 ± 0.31
40% W	48.17 ± 0.53	38.03 ± 0.53	34.76 ± 0.71	32.52 ± 0.28	30.31 ± 0.59
48% W	47.20 ± 1.06	41.74 ± 0.70	34.49 ± 0.21	32.10 ± 1.11	30.92 ± 0.92

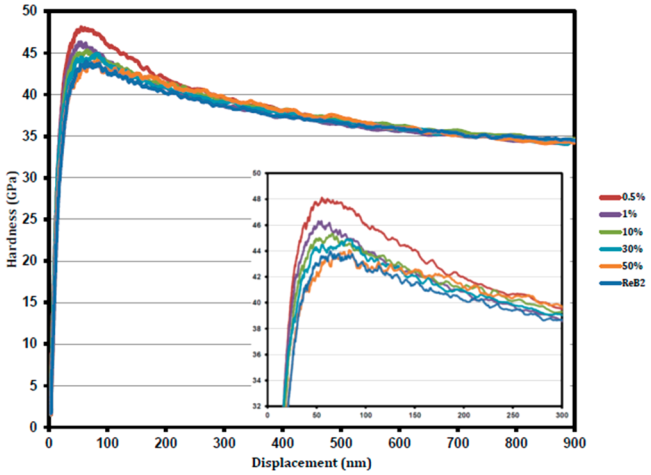

Figure 8. Nanoindentation hardness versus displacement curves for several concentrations of tungsten dissolved in ReB_2. Inset: Cropped view of the first 300 nm of indentation into the sample surface. All of the solid solutions tested maintained hardness values greater than 40 GPa until at least several hundred nanometers of penetration depth, further indicating superhardness.

Table 4. Nanoindentation Hardness at Selected Penetration Depths and Average over the Range from 60 to 900 nm

	nanoindentation hardness (GPa)			
composition	at 60 nm	at 250 nm	at 900 nm	avg (60–900 nm)
ReB_2	43.39	39.43	34.48	39.44
0.5% W	47.81	40.66	34.25	41.14
1% W	45.88	39.76	34.16	40.00
10% W	44.97	40.17	34.64	40.23
30% W	43.97	39.86	34.11	39.94
48% W	43.37	40.42	34.29	39.96

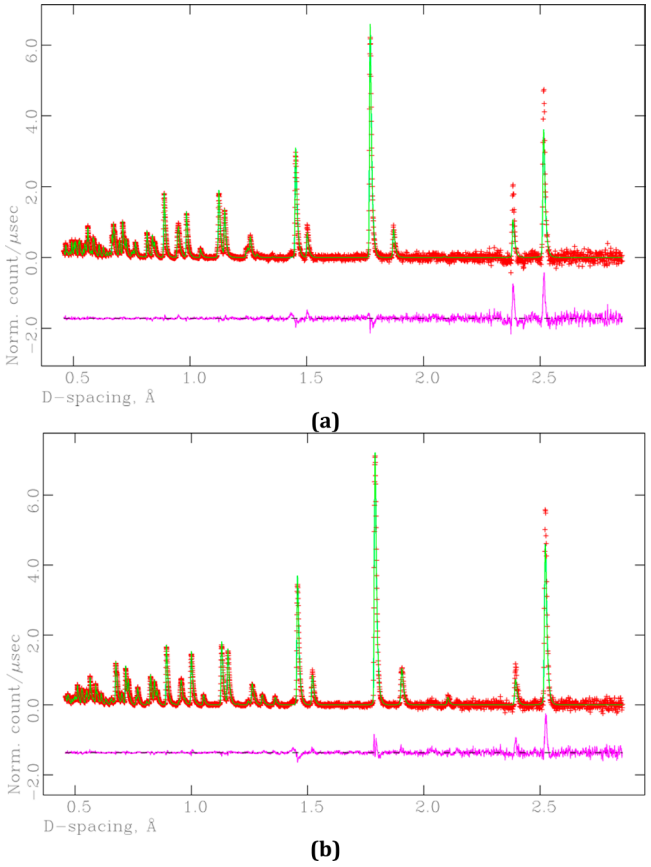

Figure 9. TOF-neutron powder diffraction refinement fit for (a) ReB_2 [statistics: R_{wp} = 1.40%, R_{wp} (background subtracted) = 1.91%, R^2_{free} = 3.41%, χ^2 = 1.731] and (b) $Re_{0.52}W_{0.48}B_2$ [statistics: R_{wp} = 1.77%, R_{wp} (background subtracted) = 2.41%, R^2_{free} = 2.44%, χ^2 = 2.023]. Red (+), observed; green (−), calculated; magenta (−), difference. The background is subtracted for clarity.

presence of WO_3. From the isothermal data at 1000 °C (lower inset of Figure 11), it may be inferred that the formation of the boron oxidation product (B_2O_3 glass) offers relatively little protection against high-temperature oxidation, as the samples continue to decompose nearly linearly at this temperature.

Whereas the boron network in AlB_2-type borides is formed by filling the interstices of a primitive hexagonal arrangement of metal atoms, ReB_2-type borides are based on an expanded hexagonal-close-packed metal lattice. From Figure 1, it is clear that one consequence of this atomic arrangement is a greater molar volumetric increase upon the addition of B to the pure metal to form ReB_2-type borides than to form AlB_2-structured compounds. For example, from Ti to TiB_2, the lattice parameters increase from a = 2.951 Å and c = 4.684 Å[53] to a = 3.024 Å and c = 3.154 Å,[54] whereas for Re to ReB_2, the parameter increase is from a = 2.76 Å and c = 4.458 Å[55] to a = 2.90 Å and c = 7.747 Å. In the case of titanium, these values correspond to a 2.47% increase in the metal–metal contact distance in a and an 8.90% increase in contact distance in c. By contrast, in the case of rhenium, 5.07 and 49.5% increases are observed along a and c, respectively.

DOI: 10.1021/jacs.6b08616
J. Am. Chem. Soc. 2016, 138, 14398–14408

Table 5. Crystallographic Data for ReB_2 from TOF-Neutron Diffraction

ReB_2									
crystal system							hexagonal		
space group							$P6_3/mmc$		
lattice parameters									
$a = b$ (Å)							2.900468(24)		
c (Å)							7.47734(10)		
V (Å^3)							54.4771(10)		
calculated density (g/cm^3)									
$R_{wp\text{-}b}$							1.91%		
χ^2							1.731		
ReB_2	mult.	symm.	x	y	z	frac.	$U_{11=22}$	U_{33}	U_{12}
Re	2	$-6m2$	1/3	2/3	1/4	1.00	0.00249(3)	0.00309(7)	0.00124(2)
B	4	$3m$	1/3	2/3	0.54805(5)	1.00	0.00559(5)	0.00630(8)	0.00100(2)

Table 6. Crystallographic Data for $Re_{0.52}W_{0.48}B_2$ from TOF-Neutron Diffraction

$Re_{0.52}W_{0.48}B_2$									
crystal system							hexagonal		
space group							$P6_3/mmc$		
lattice parameters									
$a = b$ (Å)							2.909085(21)		
c (Å)							7.61009(10)		
V (Å^3)							55.7742(9)		
calculated density (g/cm^3)									
$R_{wp\text{-}b}$							2.41%		
χ^2							2.023		
$Re_{0.52}W_{0.48}B_2$	mult.	symm.	x	y	z	frac.	$U_{11=22}$	U_{33}	U_{12}
Re	2	$-6m2$	1/3	2/3	1/4	0.52	0.00088(4)	0.00084(7)	0.00044(2)
B	4	$3m$	1/3	2/3	0.54403(4)	1.00	0.00439(3)	0.00356(6)	0.00219(2)
W	2	$-6m2$	1/3	2/3	1/4	0.48	0.00088(4)	0.00084(7)	0.00044(2)

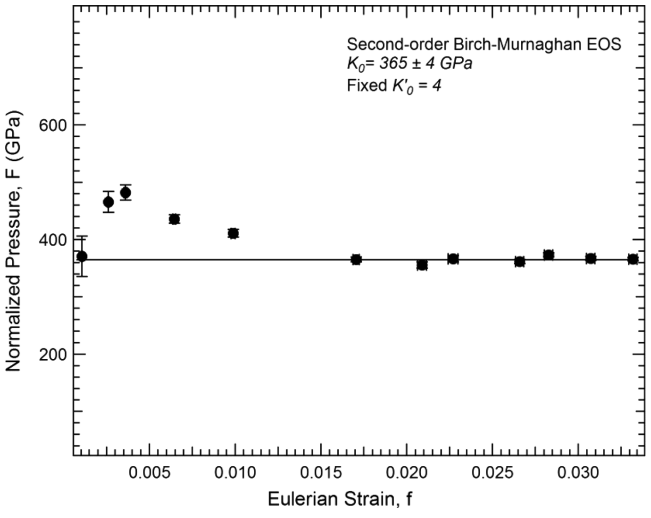

Figure 10. Compression data for $Re_{0.52}W_{0.48}B_2$ compressed under nonhydrostatic conditions and collected at φ = 54.7° to simulate hydrostatic conditions. The data are plotted in terms of normalized pressure and Eulerian strain. The straight line is a second-order fit to the Birch–Murnaghan equation of state; the variation from the trend line is commonly found at low pressures due to incomplete sample compaction.

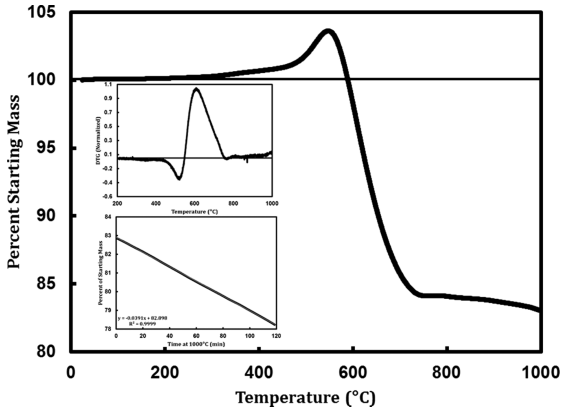

Figure 11. Percent mass versus temperature plot from the data obtained by thermogravimetric analysis (TGA) of a powdered (−325 mesh) sample containing 25 atom % tungsten under ambient air. The sample is stable to ≈520 °C before first gaining mass (due to the formation of WO_3/B_2O_3) and then rapidly losing mass at ≈610 °C (due to the volatilization of Re_2O_7). There does not appear to be any thermal stability enhancement from the addition of tungsten to ReB_2 (cf. Levine et al.[10]). Upper Inset: Normalized differential thermogravimetric (derivative) of the above data. Lower Inset: Rate of mass loss is nearly linear with time at 1000 °C, showing that the sample rapidly reaches a steady state of oxidation. It is likely that B_2O_3 acts as a flux for Re_2O_7 rather than as an oxygen barrier. The rate law equation is shown in the lower left corner.

Therefore, one may conclude that borides of the AlB_2 type can be thought of as relatively true interstitial compounds that obey the Hume-Rothery[56] rules for their formation, whereas borides of the ReB_2 type represent a distinctly layered structure with the insertion of puckered boron nets behaving as though an additional layer of metal had been added. Alternatively, in accordance with the qualitative interpretation offered by Pauling,[57] the *small* increase in metal–metal distance for the

DOI: 10.1021/jacs.6b08616
J. Am. Chem. Soc. 2016, 138, 14398–14408

AlB_2 structure type indicates a *large* degree of metal−metal bonding (at the expense of metal−boron bonding), whereas the much larger increases in compounds of the ReB_2 structure type indicate that metal−metal bonding is virtually eliminated in the *c*-direction and replaced with metal−boron covalent bonds.

This interpretation is further corroborated by the fact that the boron−boron bond distances increase from 1.75 Å in TiB_2 (an example of an AlB_2-structured compound) to 1.83 Å in ReB_2, indicating a decrease in B−B bond order going from planar boron "sheets" to "puckered" boron nets and therefore a concomitant increase in bond order from boron to metal (assuming valence is maintained).[58] Electronic calculations on ReB_2 have shown exactly this effect, with significant electron density localized between boron and rhenium, which has also been used to explain the extremely high hardness of this compound.[23,36,59] The extreme change in packing density between the two boride types is not detrimental to the hardness of the larger-volume ReB_2-type compounds but rather is a consequence of the covalency that gives rise to the high hardness. Thus, the fact that the lattice parameters for $ReWB_2$ solid solutions increase with increasing tungsten is not necessarily an indication of lowered hardness as long as metal−boron covalency is maintained or increases, and this is strongly suggested by our results.

One may hypothesize, therefore, that other compounds with the ReB_2 structure type might also be superhard. This does indeed appear to be the case as, for example, Du et al. have studied the mechanical properties of $W_{0.5}Os_{0.5}B_2$ (a = 2.913 Å, c = 7.566 Å), a ternary compound taking the ReB_2 structure, and measured a low load (0.49 N) hardness of 40.4 ± 1.3 GPa and a calculated bulk modulus of 354 GPa.[37] Additionally, recent work by Tao et al. has examined the MoB_2 system, where there are two structure types available depending on synthetic conditions.[60] Here, the structure with more puckering in the boron sheets is found to be harder than the lower-volume AlB_2-type structure. The reported high load (9.8 N) hardness values for AlB_2-type MoB_2 and "Mo_2B_4"-type MoB_2 are 15.2 and 22.0 GPa, respectively, which is a relatively drastic difference of 44.7%.[60] Given that the reported hardness of "W_2B_4"-type WB_2 is 26.1 GPa (0.98 N),[61] an additional 44.7% increase of hardness would result in a compound having a hardness of approximately 37.8 GPa, which is nearly superhard.

Indeed, ReB_2-structured WB_2 has previously been proposed as a candidate hard or superhard compound.[23,31] Chen et al. predicted from *ab initio* calculations that ReB_2-structured WB_2 should be stable versus the AlB_2-structured form under ambient conditions.[36] The calculated shear modulus reported for this structural form is 273−294 GPa based on GGA and LDA approximations, respectively (cf. 271.6−302 GPa for ReB_2, as determined experimentally[62,63]). Assuming that the correlation between shear modulus and indentation hardness holds,[64] this may be interpreted as a prediction that the hardness of ReB_2-structured WB_2 should have comparable hardness to that of native ReB_2. This hypothesis was later partially supported by Zhong et al., who used the Voigt−Reuss−Hill (VRH) approximation to calculate shear moduli of 253 and 291 GPa and employed a semiempirical method to estimated hardness values of 35.7 and 39.1 GPa for ReB_2-structured WB_2 and native ReB_2, respectively.[31]

Unfortunately, WB_2 takes the "W_2B_4"-type structure under ambient conditions, and a material with the ReB_2-structure polymorph has never been isolated at that stoichiometry. However, some speculation has been offered from theoretical calculations about the properties of W/ReB_2 solid solutions, and these compounds were anticipated to also be superhard.[20,32,37] The estimated values for the hardness of $W_{0.5}Re_{0.5}B_2$ is 40.1 GPa and the bulk modulus is 354 GPa according to Du et al.;[37] and similar hardness of 40.9 GPa was calculated by Ivanovskii.[65] Our results are in excellent agreement with these claims, as the experimentally determined values for the hardness of $Re_{0.52}W_{0.48}B_2$ are 41.7 ± 0.7 GPa (0.98 N) from microindentation and 39.96 GPa (average) from nanoindentation. The measured bulk modulus of 365 ± 4 GPa for the $Re_{0.52}W_{0.48}B_2$ composition is slightly higher than the calculated value of 354 GPa, but it is in the right range. While there are some discrepancies in the lattice parameters between the predicted values of a = 2.88 Å c = 7.57 Å according to Du[37] and a = 2.8702 Å and c = 7.5224 Å according to Tu et al.[32] and our experimentally determined values of a = 2.9076 Å and c = 7.6076 Å for ∼50 atom % W, the excellent qualitative agreement between the sets of results would seem to indicate that computational methods have quite some value in the prediction of properties of hard materials.

Tu et al. further predicted peaks in the hardness of tungsten/rhenium diboride solid solutions at both 10 atom % W and 60 atom % tungsten, predictions that agree well with our experimental results, especially if 60% is taken to correspond to our data at 48 atom %. The slight variations in hardness that we observe in the range from 10 to 50 atom % W can likely be ascribed to subtle electronic effects. However, none of the previously described theoretical works predict the relatively large increase in hardness that we observe for small amounts of additional tungsten in the range of 0.5−2 atom %. The likely cause of this discrepancy is that the theoretical calculations take for granted the perfect stoichiometric ratio, atomic regularity, and homogeneity that may only exist in an ideal compound. All real samples should be expected to have some slight deviations from perfect stoichiometry, many of which will manifest as slight strains on the lattice. A strained crystalline lattice should be expected to contribute to the hardness of the compound. The addition of very small amounts of tungsten may enter the crystalline structure of ReB_2 in such a way as to compensate for these strains and may therefore exert a disproportionately large effect on the measured hardness of the compound. One would not expect to be able to calculate this sort of extrinsic factor given the assumptions made in the theoretical calculations.

Recent interest in the metal-boride field has grown, in part due to the desire for further understanding of the inherent properties of the materials but also because of the potential applications of these materials. Theoretical calculations are beginning to meet experimental results more frequently, and with the increasing accuracy of these computational predictions, they are becoming useful partners and guides for synthesis studies. We note, however, that from atomic-level interactions to mesoscale and continuum properties, many intricacies remain for these borides. Despite this excellent agreement with first-principles predictions, the metal-boride family of materials still has many open questions to be answered.[66−68]

As far as we are aware, the only other experimental work on these solid solutions was executed as part of a phase-diagrammatic study by Kuz'ma et al., who reported a maximum solubility limit of $Re_{0.81}W_{0.19}B_2$ with lattice parameters a = 2.910 Å and c = 7.590 Å.[19] On the basis of the axial ratio (2.6082), these values correspond well to values along our curve for a boride of formula $Re_{0.65}W_{0.35}B_2$. The discrepancy in the atomic fraction is likely due to poor optimization of the compositions for the samples in the Kuz'ma study, given that most samples prepared

DOI: 10.1021/jacs.6b08616
J. Am. Chem. Soc. 2016, 138, 14398−14408

in that work were multiphase ingots, making it much more difficult to estimate the atomic ratios in each phase of the sample. A plausible contribution to the difference between our estimates for maximum tungsten solubility is a slight boron deficiency in the compounds synthesized in previous works. Over the course of optimizing our own synthetic procedure, we have found that a slight excess of boron is necessary to ensure the complete formation of the ReB_2 structured compound. It is important to note that ratios of boron to metal of less than approximately 2.2:1 (B:M) during synthesis appear to encourage the formation of the "W_2B_4" phase.

CONCLUSIONS

In this work, we have successfully synthesized solid solutions of tungsten in ReB_2 using an electric-arc furnace. The solubility limit for tungsten in ReB_2 is nearly 50 atom % (maximum composition reported here is 48%), indicating a very high degree of solubility. The lattice parameters for the solid solutions vary linearly along both the *a*- and *c*-axes with increasing tungsten content. The solid solutions are statistically random up to and including the limiting composition, according to both X-ray and neutron diffraction. All of the compositions tested within the range from 0 to 48 atom % W are superhard according to analyses of both micro- and nanoindentation data, and the bulk modulus of 48% W solid solution is nearly identical to that of the pure ReB_2 material. These results further indicate that ReB_2-structured compounds are superhard and may warrant further studies into additional solid solutions or ternary compounds taking this structure type.

AUTHOR INFORMATION

Corresponding Author

*kaner@chem.ucla.edu

Author Contributions

⊥A.T.L. and C.L.T. contributed equally to this work.

Notes

The authors declare no competing financial interest.

ACKNOWLEDGMENTS

The authors thank Drs. Sven Vogel, Luke Deamon, and Helmut Reike at the Lujan Center of the Los Alamos National Laboratory for their help with neutron diffraction experiments, Prof. Benjamin M. Wu at the UCLA Department of Materials Science and Engineering for use of his microindentation system, Dr. Miao Xie for assistance with microindentation measurements, and Prof. Jeng-Ming Yang at the UCLA Department of Materials Science and Engineering for use of his nanoindentation instrumentation. Ceradyne (Costa Mesa, CA) generously provided materials support through their provision of isotopically enriched ^{11}B, which we gratefully acknowledge. This work was funded by the National Science Foundation under grant number DMR-1506860 (S.H.T. and R.B.K.); additionally, R.M. thanks VCU for their gracious support (startup grant 137422). Work at LANSCE was supported by the Department of Energy under grant number 20112198. Crystal-chemical illustrations in this work were made using the VESTA software package. The authors thank J. Yuan, M. Kunz, and A. MacDowell for help preparing the boron-epoxy gaskets at Lawrence Berkeley National Laboratory (LBNL) beamline 12.2.2. We also thank Professor H.-R. Wenk for technical support. Radial diffraction experiments were performed at Advanced Light Source 12.2.2 (LBNL). Advanced Light Source is supported by the Director, Office of Science, Office of Basic Energy Sciences, of the U.S. Department of Energy under Contract No. DEAC02-05CH11231. Radial diffraction studies were partly supported by COMPRES, the Consortium for Materials Properties Research in Earth Sciences, under NSF Cooperative Agreement EAR-1606856.

REFERENCES

(1) *Boron and Refractory Borides*; Matkovich, V. I., Ed.; Springer Berlin Heidelberg: Berlin, 1977.
(2) Mohammadi, R.; Kaner, R. B. Superhard Materials. In *Encyclopedia of Inorganic and Bioinorganic Chemistry*; Scott, R. A., Ed.; John Wiley & Sons, Ltd: Chichester, UK, 2011.
(3) Sung, C.-M.; Sung, M. *Mater. Chem. Phys.* **1996**, *43*, 1−18.
(4) Brazhkin, V. V.; Lyapin, A. G.; Hemley, R. J. *Philos. Mag. A* **2002**, *82*, 231−253.
(5) Weinberger, M. B.; Levine, J. B.; Chung, H.; Cumberland, R. W.; Rasool, H. I.; Yang, J.-M.; Kaner, R. B.; Tolbert, S. H. *Chem. Mater.* **2009**, *21*, 1915−1921.
(6) Gilman, J. J.; Cumberland, R. W.; Kaner, R. B. *Int. J. Refract. Hard Met.* **2006**, *24*, 1−5.
(7) Kaner, R. B.; Gilman, J. J.; Tolbert, S. H. *Science* **2005**, *308*, 1268−1269.
(8) Albert, B.; Hillebrecht, H. *Angew. Chem., Int. Ed.* **2009**, *48*, 8640−8668.
(9) Fehlner, T. P. *J. Solid State Chem.* **2000**, *154*, 110−113.
(10) Levine, J. B.; Nguyen, S. L.; Rasool, H. I.; Wright, J. A.; Brown, S. E.; Kaner, R. B. *J. Am. Chem. Soc.* **2008**, *130*, 16953−16958.
(11) Chung, H.-Y.; Weinberger, M. B.; Levine, J. B.; Cumberland, R. W.; Kavner, A.; Yang, J.-M.; Tolbert, S. H.; Kaner, R. B. *Science* **2007**, *316*, 436−439.
(12) Mohammadi, R.; Xie, M.; Lech, A. T.; Turner, C. L.; Kavner, A.; Tolbert, S. H.; Kaner, R. B. *J. Am. Chem. Soc.* **2012**, *134*, 20660−20668.
(13) Mohammadi, R.; Lech, A. T.; Xie, M.; Weaver, B. E.; Yeung, M. T.; Tolbert, S. H.; Kaner, R. B. *Proc. Natl. Acad. Sci. USA* **2011**, *108*, 10958−10962.
(14) Shibuya, M.; Kawata, M.; Ohyanagi, M.; Munir, Z. A. *J. Am. Ceram. Soc.* **2003**, *86*, 706−710.
(15) Rogl, P.; Nowotny, H.; Benesovsky, F. *Monatsh. Chem.* **1970**, *101*, 27−31.
(16) Rogl, P.; Nowotny, H.; Benesovsky, F. *Monatsh. Chem.* **1970**, *101*, 850−854.
(17) Rogl, P.; Rudy, E. *J. Solid State Chem.* **1978**, *24*, 175−181.
(18) Zeiringer, I.; Rogl, P.; Grytsiv, A.; Polt, J.; Bauer, E.; Giester, G. *J. Phase Equilib. Diffus.* **2014**, *35*, 384−395.
(19) Kuz'ma, Y. B.; Lakh, V. I.; Stadnyk, B. I.; Voroshilov, Y. V. *Sov. Powder Metall. Met. Ceram.* **1968**, *7*, 462−466.
(20) Lin, F.; Wu, K.; He, J.; Sa, R.; Li, Q.; Wei, Y. *Chem. Phys. Lett.* **2010**, *494*, 31−36.
(21) Wang, Y. X. *Appl. Phys. Lett.* **2007**, *91*, 101904.
(22) Šimůnek, A. *Phys. Rev. B: Condens. Matter Mater. Phys.* **2009**, *80*, 060103.
(23) Hao, X.; Xu, Y.; Wu, Z.; Zhou, D.; Liu, X.; Cao, X.; Meng, J. *Phys. Rev. B: Condens. Matter Mater. Phys.* **2006**, *74*, 224112.
(24) Aydin, S.; Simsek, M. *Phys. Rev. B: Condens. Matter Mater. Phys.* **2009**, *80*, 134107.
(25) Lazar, P.; Chen, X.-Q.; Podloucky, R. *Phys. Rev. B: Condens. Matter Mater. Phys.* **2009**, *80*, 012103.
(26) Zhong, M.-M.; Kuang, X.-Y.; Wang, Z.-H.; Shao, P.; Ding, L.-P.; Huang, X.-F. *J. Alloys Compd.* **2013**, *581*, 206−212.
(27) Liang, Y.; Li, A.; Zhao, J.; Zhang, W. *Mod. Phys. Lett. B* **2009**, *23*, 1281−1290.
(28) Zhou, W.; Wu, H.; Yildirim, T. *Phys. Rev. B: Condens. Matter Mater. Phys.* **2007**, *76*, 184113.
(29) Chen, W.; Jiang, J. Z. *Solid State Commun.* **2010**, *150*, 2093−2096.
(30) Soto, G.; Moreno-Armenta, M. G.; Reyes-Serrato, A. *Comput. Mater. Sci.* **2008**, *44*, 628−634.

DOI: 10.1021/jacs.6b08616
J. Am. Chem. Soc. 2016, 138, 14398−14408

(31) Zhong, M.-M.; Kuang, X.; Wang, Z.-H.; Shao, P.; Ding, L.-P.; Huang, X.-F. *J. Phys. Chem. C* **2013**, *117*, 10643−10652.
(32) Tu, Y.; Wang, Y. *Solid State Commun.* **2011**, *151*, 238−241.
(33) Tian, Y.; Xu, B.; Zhao, Z. *Int. J. Refract. Hard Met.* **2012**, *33*, 93−106.
(34) Gao, F. M.; Gao, L. H. *J. Superhard Mater.* **2010**, *32*, 148−166.
(35) Šimůnek, A. *Phys. Rev. B: Condens. Matter Mater. Phys.* **2007**, *75*, 172108.
(36) Chen, X.-Q.; Fu, C.; Krčmar, M.; Painter, G. *Phys. Rev. Lett.* **2008**, *100*, 196403.
(37) Du, X. P.; Wang, Y. X. *Phys. Status Solidi RRL* **2009**, *3*, 106−108.
(38) Ivanovskii, A. L. *Prog. Mater. Sci.* **2012**, *57*, 184−228.
(39) Hölzer, G.; Fritsch, M.; Deutsch, M.; Härtwig, J.; Förster, E. *Phys. Rev. A: At., Mol., Opt. Phys.* **1997**, *56*, 4554−4568.
(40) Toby, B. H. *J. Appl. Crystallogr.* **2001**, *34*, 210−213.
(41) Larson, A. C.; Von Dreele, R. B. *Report LAUR 86-748*; Los Alamos National Laboratory: Los Alamos, NM, 2000.
(42) Oliver, W. C.; Pharr, G. M. *J. Mater. Res.* **1992**, *7*, 1564−1583.
(43) Hemley, R. J.; Mao, H. K.; Shen, G.; Badro, J.; Gillet, P.; Hanfland, M.; Häusermann, D. *Science* **1997**, *276* (5316), 1242−1245.
(44) Hammersley, A. P.; Svensson, S. O.; Hanfland, M.; Fitch, A. N.; Hausermann, D. *High Pressure Res.* **1996**, *14*, 235−248.
(45) Frotscher, M.; Hölzel, M.; Albert, B. *Z. Anorg. Allg. Chem.* **2010**, *636*, 1783−1786.
(46) Singh, A. K.; Mao, H. K.; Shu, J.; Hemley, R. J. *Phys. Rev. Lett.* **1998**, *80* (10), 2157.
(47) Singh, A. K. *J. Appl. Phys.* **1993**, *73*, 4278−4286.
(48) Singh, A. K.; Balasingh, C.; Mao, H.-K.; Hemley, R. J.; Shu, J. *J. Appl. Phys.* **1998**, *83*, 7567−7575.
(49) Birch, F. *J. Geophys. Res.* **1978**, *83*, 1257.
(50) Meade, C.; Jeanloz, R. *Geophys. Res. Lett.* **1990**, *17*, 1157.
(51) Yin, S.; He, D.; Xu, C.; Wang, W.; Wang, H.; Li, L.; Zhang, L.; Liu, F.; Liu, P.; Wang, Z.; Meng, C. *High Pressure Res.* **2013**, *33*, 409−417.
(52) Suzuki, Y.; Levine, J. B.; Migliori, A.; Garrett, J. D.; Kaner, R. B.; Fanelli, V. R.; Betts, J. B. *J. Acoust. Soc. Am.* **2010**, *127*, 2797.
(53) Wood, R. M. *Proc. Phys. Soc., London* **1962**, *80*, 783−786.
(54) Deligoz, E.; Colakoglu, K.; Ciftci, Y. O. *Solid State Commun.* **2009**, *149*, 1843−1848.
(55) Swanson, H.; Fuyat, R. K.; Ugrinic, G. M. *Standard X-ray Diffraction Powder Patterns*; U.S. Dept. of Commerce, National Bureau of Standards: Washington, DC, 1954.
(56) Hume-Rothery, W. *Philos. Mag. Ser. 7* **1953**, *44*, 1154−1160.
(57) Pauling, L. *J. Am. Chem. Soc.* **1947**, *69*, 542−553.
(58) Rundle, R. E. *Acta Crystallogr.* **1948**, *1*, 180−187.
(59) Wang, J.; Wang, Y.-J. *J. Appl. Phys.* **2009**, *105*, 083539.
(60) Tao, Q.; Zhao, X.; Chen, Y.; Li, J. J.; Li, Q.; Ma, Y.; Cui, T.; Zhu, P.; Wang, X. *RSC Adv.* **2013**, *3*, 18317.
(61) Okada, S.; Kudou, K.; Lundström, T. *Jpn. J. Appl. Phys.* **1995**, *34*, 226−231.
(62) Suzuki, Y.; Levine, J. B.; Migliori, A.; Garrett, J. D.; Kaner, R. B.; Fanelli, V. R.; Betts, J. B. *J. Acoust. Soc. Am.* **2010**, *127*, 2797−2801.
(63) Chung, H.-Y.; Weinberger, M. B.; Yang, J.-M.; Tolbert, S. H.; Kaner, R. B. *Appl. Phys. Lett.* **2008**, *92*, 261904.
(64) Teter, D. M. *MRS Bull.* **1998**, *23*, 22−27.
(65) Ivanovskii, A. L. *J. Superhard Mater.* **2012**, *34*, 75−80.
(66) Chrzanowska, J.; Hoffman, J.; Denis, P.; Giżyński, M.; Mościcki, T. *Surf. Coat. Technol.* **2015**, *277*, 15−22.
(67) Koumoulis, D.; Turner, C. L.; Taylor, R. E.; Kaner, R. B. *J. Phys. Chem. C* **2016**, *120*, 2901−2907.
(68) Maździarz, M.; Mościcki, T. *J. Alloys Compd.* **2016**, *657*, 878−888.

DOI: 10.1021/jacs.6b08616
J. Am. Chem. Soc. 2016, 138, 14398−14408